Abstract: We report new laser and nonlinear-laser properties of Nd^{3+}-ion doped and undoped orthorhombic calcium niobate. In particular, we show that: Nd^{3+}:$Ca(NbO_3)_2$ is a promising gain medium for LD-pumped microchip lasers and undoped $Ca(NbO_3)_2$ can give rise to high-order lasing covering more than two-octave Stokes and anti-Stokes frequency comb in the visible and near-IR region. We measured also the main spectroscopic intensity characteristics related to the observed laser performance and identified their physical nature.

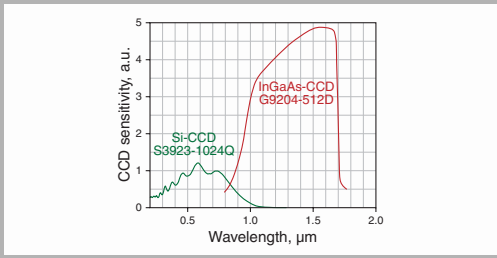

Used sensors provide good enough sensitivity in a very wide spectral range

Laser and nonlinear-laser properties of undoped and Nd^{3+}-doped orthorhombic $Ca(NbO_3)_2$ single crystals: new stimulated-emission performance and high-order picosecond stimulated Raman scattering covering more than two octave Stokes and anti-Stokes wavelengths

A.A. Kaminskii, [1,*] *J. Dong,* [2,**] *H.J. Eichler,* [3] *J. Hanuza,* [4,5] *K. Ueda,* [6] *M. Maczka,* [4] *H. Rhee,* [3] *and M. Bettinelli* [7]

[1] Institute of Crystallography, Russian Academy of Sciences, Moscow 119333, Russia
[2] Department of Electronic Engineering, School of Information Science and Technology of Xiamen University, Xiamen 361005, China
[3] Institute of Optics and Atomic Physics, Technical University of Berlin, Berlin 10623, Germany
[4] Institute of Low Temperature and Structure Research, Polish Academy of Sciences, Wroclaw 50950, Poland
[5] Department of Bioorganic Chemistry, Institute of Chemistry and Food Technology, Wroclaw University of Economics, Wroclaw 53450, Poland
[6] Institute for Laser Science, University of Electro-Communications, 182-8585 Tokyo, Japan
[7] Laboratorio di Chimica dello Stato Solido, DB, Universitá di Virona and INSTM, Verona 37134, Italy

Received: 13 July 2009, Accepted: 20 July 2009
Published online: 3 August 2009

Key words: stimulated emission; stimulated Raman scattering (SRS); $Ca(NbO_3)_2$-SRS-active crystal; Stokes and anti-Stokes comb generation; $Ca(NbO_3)_2$:Nd^{3+} laser crystal; microchip-solid-state LD-pumped laser

PACS: 42.55.Rz, 42.65.Dr, 42.65.Ky, 78.30.Jw

1. Introduction

In modern laser physics and nonlinear optics, niobium containing crystals, in spite of the limitedness of their present arsenal, play an important role (see, e.g. [1–5]. The structural diversity of these niobates provides a wide variety of physical properties which have attractive practical aspects. Among them are stimulated emission (SE) for different lasing modes with trivalent lanthnides (Ln^{3+}) and transition metal lasants, second harmonic generation (SHG), stimulated Raman scattering (SRS), numerous parametric processes, etc. (see Table 1). Due to their strong $\chi^{(2)}$- and $\chi^{(3)}$- nonlinear activity they make possible the

* Corresponding author: e-mail: kaminalex@mail.ru, ** jdong@xmu.edu.cn

Crystal	Space group	Ln^{3+} lasant [a]	Nonlinear property	SRS-active mode, cm^{-1}	Observed nonlinear-laser effects [b]	Ref. [c]
$LiNbO_3$	C_{3v}^6	Nd^{3+}, Dy^{3+}, Ho^{3+}, Er^{3+}, Tm^{3+}, Yb^{3+}	$\chi^{(2)}+\chi^{(3)}$ (polar)	490 – 628, 212 – 248, $\approx$ 152 [d]	SHG, SRS, OPO, self-FD (Nd^{3+}, Yb^{3+}), self-SFG (Nd^{3+})	[6]
$LiNbO_3$:MgO [e]	C_{3v}^6	Nd^{3+}, Er^{3+}, Yb^{3+}	$\chi^{(2)}+\chi^{(3)}$ (polar)	–	self-FD (Nd^{3+}, Yb^{3+}) [f], self-pump OPO (Nd^{3+}, Yb^{3+})	–
$LiNbGeO_5$	D_{2h}^{16}	Cr [g]	$\chi^{(3)}$	$\approx$ 786, $\approx$ 754, $\approx$ 699	SRS	[7]
$K_3Nb_3O_6(BO_3)_2$	C_{2v}^2	–	$\chi^{(2)}+\chi^{(3)}$ (polar)	$\approx$ 648, $\approx$ 324	SHG, SRS	[8]
$Ca(NbO_3)_2$	$\boldsymbol{D_{2h}^{14}}$	Pr^{3+}, **Nd^{3+}**, Ho^{3+}, Er^{3+}, Tm^{3+} [h]	$\chi^{(3)}$	**$\approx$ 904, $\approx$ 538**	**SRS**	**this work**
$Ca_{0.25}Ba_{0.75}(NbO_3)_2$	D_{2h}^{14}	Nd^{3+}	$\chi^{(3)}$	–	–	–
$\{Ca_3\}[Nb,Ga]_2(Ga_3)O_{12}$	O_h^{10}	Nd^{3+}, Er^{3+}	$\chi^{(3)}$	$\approx$ 500	SRS	[9]
$Sr_{0.4}Ba_{0.6}(NbO_3)_2$	C_{2v}^4	Nd^{3+}	$\chi^{(2)}+\chi^{(3)}$ (polar)	–	SHG, self-FD (Nd^{3+}) [i]	–
$Ba_2NaNb_5O_{15}$	C_{2v}^{11}	Nd^{3+}	$\chi^{(2)}+\chi^{(3)}$ (polar)	$\approx$ 650	SHG, SRS, self-FD (Nd^{3+})	[6,10]
$La_3Ga_{5.5}Nb_{0.5}O_{14}$	D_3^2	Nd^{3+}, Cr^{3+}	$\chi^{(2)}+\chi^{(3)}$	–	SHG, self-FD (Nd^{3+}, Cr^{3+}) [j]	–
$LaNbO_4$	C_{2h}^6	Nd^{3+}, Ho^{3+}	$\chi^{(3)}$	–	–	–

[a] More detail data on SE of lasant activator ions is available from [11].

[b] Here we used the following abbreviations:
- SHG – second harmonic generation;
- OPO – optical parametric oscillation;
- self-FD (Ln^{3+}) - self-frequency doubling, i.e. SHG from arising SE in Ln^{3+}-ion doped crystals under external non-laser and/or laser pumping;
- self-pump OPO (Nd^{3+}) - optical parametric oscillation arising from SE of Nd^{3+} lasants, which is as an internal one-micron pumping radiation;
- self-SFG is the self-sum-frequency mixing, i.e. cascaded summing parametric generation (up-conversion process) of arising secondary laser emissions (e.g., SE, Stokes and anti-Stokes lasing, as well as pumping radiation).

[c] In this table and below we used articles only in refereed journals.

[d] Including polariton modes.

[e] The Mg^{2+}(MgO) co-doped $LiNbO_3$:Nd^{3+} laser crystals for the first time were used in [12]. Other "co-activators" ZnO, Sc_2O_3, and ZrO_2 are also known.

[f] Self-FD effect under quasi-phase-matched condition was also observed in $LiNbO_3$:MgO:Yb^{3+} crystal with the periodically domain-inverted structure [13].

[g] Assumed as Cr^{4+} ions.

[h] All known laser channels documented in Table 2.

[i] Diffuse self-FD phenomenon was observed in the crystals with randomly distributed quasi-cylindrical ferroelectric domains [14]. The theory of this phenomenon was described in [15].

[j] Non-phase-matched SHG [16].

Table 1 Known nonlinear-laser niobate single crystals

availability of efficient conversion of visible and near-IR laser emission into different specific wavelengths. Therefore, it is of current interest to search and study the laser and nonlinear-laser properties of new and known undoped and Ln^{3+}-ion doped niobates.

Our present research is concerned with the detailed investigation of undoped and Nd^{3+}-ion doped orthorhombic $Ca(NbO_3)_2$ crystals. Here we present results about CW one-micron Nd^{3+}:$Ca(NbO_3)_2$ microchip laser performance with laser-diode (LD) pumping and a study of picosecond SRS in undoped $Ca(NbO_3)_2$ crystal. This investigation is a continuation of our previous spectroscopic and SE generation studies of Ln^{3+} lasants in title crystals, which are partly described in Table 2 (in addition, see also [4]). It should be noted here that $Ca(NbO_3)_2$ was the seventh laser host-crystal (after CaF_2, SrF_2, BaF_2, LaF_3, $CaWO_4$, and $SrMoO_4$) for Ln^{3+} lasants [26].

2. Crystals for investigations

Both undoped and neodymium activated $Ca(NbO_3)_2$ (or $CaNb_2O_6$) crystals were grown by the usual Czochralski technique. Good optical quality calcium niobate single crystals doped with $\approx$2% Nd^{3+} lasants by weight in

Pr^{3+}	Nd^{3+}	Ho^{3+}	Er^{3+}	Tm^{3+}
$^1D_2 \rightarrow {}^3F_4$ [a]	$^4F_{3/2} \rightarrow {}^4I_{11/2}$ [b]	$^5I_7 \rightarrow {}^5I_8$	$^4S_{3/2} \rightarrow {}^4I_{9/2}$	$^3H_4 \rightarrow {}^3H_6$
300 K, Xe 1.0664 μm [17]	300 K, Xe, LD [c] 1.0615 μm [18]	$\approx$ 90 K, Xe $\approx$ 2.047 μm [19]	$\approx$ 110 K, Xe 1.7410 μm [20]	77 K, Xe $\approx$ 1.91 μm [19]
77 K, Xe 1.0662 μm [17]	$\approx$ 650 K, Xe 1.0625 μm [21]			
	77 K, Xe 1.0612 μm [18,22]			
$^3P_0 \rightarrow {}^3H_6$	$^4F_{3/2} \rightarrow {}^4I_{13/2}$		$^4I_{11/2} \rightarrow {}^4I_{13/2}$	
$\approx$ 110 K, Xe 0.6105 μm [20]	300 K, Xe 1.3380 and 1.3425 μm [23]		$\approx$ 110 K, Xe 2.7175 μm [20]	
	77 K, Xe 1.3370 and 1.3415 μm [23]			
			77 K, Xe $\approx$ 1.61 μm [17] [d]	

[a] Excited under Xe-flashlamp pumping pulsed SE at $\approx$ 1.04 μm wavelength of Pr^{3+} ions at 77 K was wrongly assigned to the $^4F_{3/2} \rightarrow {}^4I_{9/2}$ channel [19]. A subsequent correct identification made in [24] showed that this SE related to the $^1D_2 \rightarrow {}^3F_4$ channel.

[b] Recorded room-temperature pulsed SE at 1.060 μm wavelength of Nd^{3+} ions was wrongly assigned to the $^4F_{3/2} \rightarrow {}^4I_{9/2}$ channel [19].

[c] In the SE spectrum of a crystal $Ca(NbO_3)_2$:Nd^{3+} grown without charge compensators besides the generation line at 1.0612 μm wavelength of the "main" activator center, several lines related to the N-type satellite Nd^{3+} lasing centers are also manifested (at 1.0614 μm for the N_1 center, at 1.0626 μm – N_2 center, and 1.0588 μm – N_3 center). All these SE wavelengths (see Fig. 7 in [22]) were recorded by the use of combined active media [25] on the base of $Ca(NbO_3)_2$:Nd^{3+} + BaF_2 - LaF_3:Nd^{3+} or $Ca(NbO_3)_2$:Nd^{3+}+Nd-glass.

[d] Pulsed SE of Er^{3+} ions was recorded at 77 K with Xe-flashlamp pumping at $\approx$ 1.61 μm wavelength without identification of the laser channel.

Table 2 Known SE channels of the orthorhombic $Ca(NbO_3)_2$ single crystals doped with Ln^{3+} lasants (Ln^{3+} = Pr^{3+}, Nd^{3+}, Ho^{3+}, Er^{3+}, and Tm^{3+})

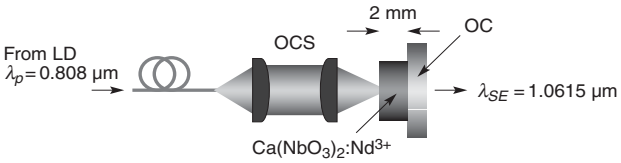

Figure 1 (online color at www.lphys.org) Schematic diagram of the 0.808-μm LD-pumped Nd^{3+}:$Ca(NbO_3)_2$ microchip CW laser (see also text)

the melt were obtained with the stoichiometric amounts of Ti^{4+} charge compensators. All calcium niobates were pulled (rate $\approx$ 6 mm/h and rotation $\approx$ 30 min^{-1}) in air using an Ir crucible. These crystals were used to fabricate polished samples for laser, nonlinear-laser, and spectroscopic measurements. The crystallographic and some physical properties of the niobates studied are listed in Table 3.

3. CW lasing of Nd^{3+}:$Ca(NbO_3)_2$ single crystal with LD pumping

The schematic diagram of our microchip laser is shown in Fig. 1. One surface of the $Ca(NbO_3)_2$:Nd^{3+} gain element in the form of crystal plate is anti-reflection-coated at 0.808 μm and highly reflecting at 1.064 μm wavelength to act as a cavity mirror of the laser. The other surface of the $Ca(NbO_3)_2$:Nd^{3+} crystal plate is anti-reflection-coated to reduce the cavity loss at SE wavelength. Four plane-parallel mirrors were used as output couplers (OC) with different transmissions of 5%, 10%, 15%, and 20% at 1.0615 μm. The overall cavity length was about 2 mm. A 7-W fiber-coupled 0.808 μm LD with a core diameter of 100 μm and numerical aperture of 0.2 was used as the pump source. Two lenses of 8-mm focal length were used to focus the pump beam on the crystal rear surface and to produce a pump light footprint in the crystal of about 100 μm in diameter. About 95% of the total pumping power is incident on the $Ca(NbO_3)_2$:Nd^{3+} crystal plate after the optical coupling system (OCS). Unfor-

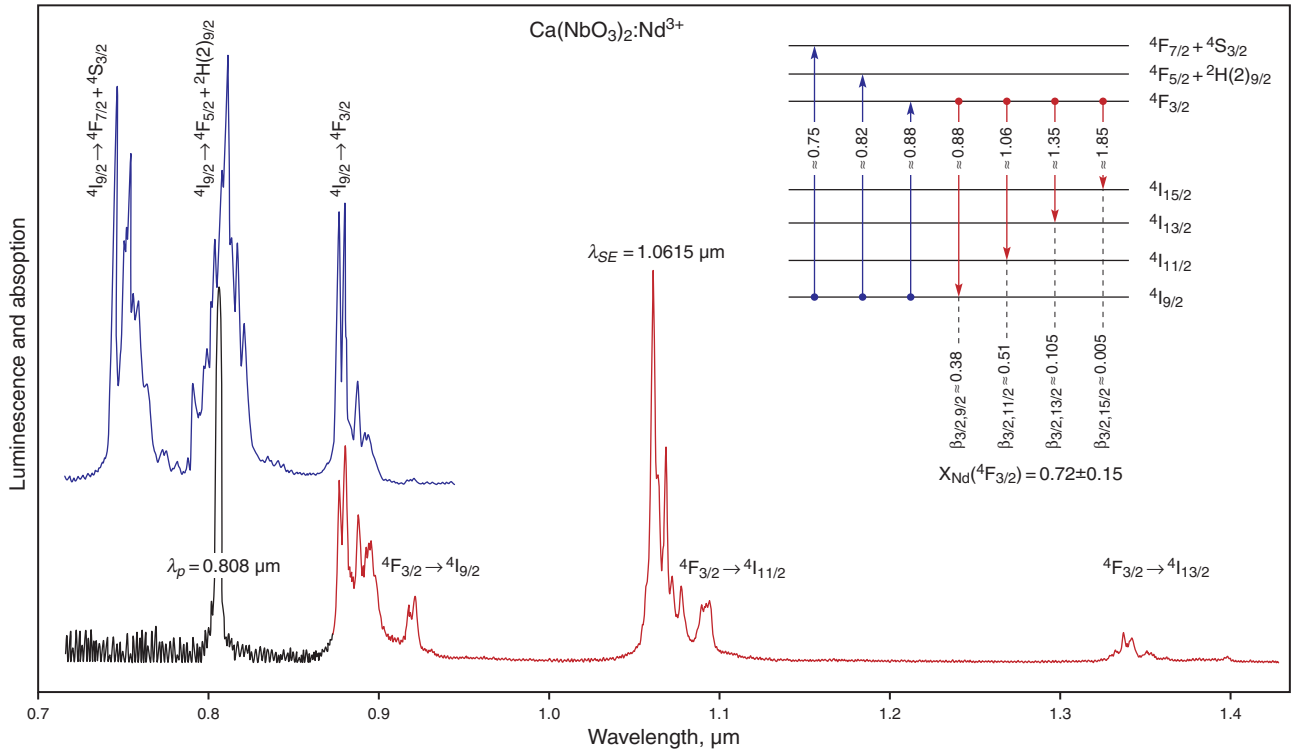

Figure 2 (online color at www.lphys.org) Spectroscopic map explaining the $^4F_{3/2} \rightarrow {}^4I_{9/2-15/2}$ luminescence of Nd^{3+} ions in a orthorhombic $Ca(NbO_3)_2$ crystal with 808-μm LD-excitation (see also text)

tunately, in the used excitation condition, as will be seen from Fig. 2, CW LD-emission at $\lambda_p = 0.808$ μm wavelength is not fully matched with the maximum of the peak of pumping band-area which related to intermanifold absorption $^4F_{3/2} \rightarrow {}^4F_{5/2}+{}^2H(2)_{9/2}$ transition. The developed microchip laser was operated at room temperature without active cooling of the crystal element.

The CW input-output dependences of microchip $Ca(NbO_3)_2$:Nd^{3+} laser as a function of the absorbed pump power for different OC are shown in Fig. 3a. The excitation threshold was approximately the same of ≈ 180 mW when the transmissions of the OC are 5%, 10%, and 15%. At $T_{OC} = 20\%$ it was about 250 mW. As seen, the output power increases linearly with the absorbed pump power for different transmissions of the OC. The maximum output power of ≈ 1.4 W was achieved with $T_{OC} = 10\%$ when the absorbed pump power was 4.55 W, in this case the optical-to-optical efficiency is as high as 31%. The measured CW lasing efficiencies for other transmission of OC are given in Fig. 3a.

The $Ca(NbO_3)_2$:Nd^{3+} microchip SE was analyzed by using an ANDO AQ6317 optical spectrum analyzer. As may be seen from Fig. 3b, the laser spectra of our laser indicate that several longitudinal modes oscillate simultaneously for different OC. For $T_{OC} = 5\%$, three longitudinal modes oscillate at 1.0615 μm when the pump power is just above threshold, the number of the longitudinal modes increase with the absorbed pump power, for example, five longitudinal modes oscillate when the pump power is ≈ 3 W. The generation wavelength shifts to longer wavelength with absorbed pump power, which is related to the SE spectral shift to longer wavelength with increasing temperature of the lasing crystal. This effect related to the electron-phonon interaction active in a $Ca(NbO_3)_2$:Nd^{3+} crystal was investigated in detail many years ago using special laser measurements conducted over a wide temperature range (from 77 K to 630 K) [22]. It should be noted here that the same behaviour was observed in $Y_3Al_5O_{12}$:Nd^{3+} microchip laser as reported in [37]. Similar cavity mode behaviours in our $Ca(NbO_3)_2$:Nd^{3+} microchip laser were found with different transmissions of OC, as indicated in Fig. 3b. The separation of each longitudinal mode under different pump power was measured to be $\Delta\lambda \approx 1.35$ Å. In agreement with [38] this value should be estimate by the simple relation $\Delta\lambda = \lambda_{SE}^2/2L_c$, where L_c is the optical length of the laser cavity with regards to the refractive index of the crystal. For 2-mm thick $Ca(NbO_3)_2$:Nd^{3+} planar-parallel gain crystal studied here, $\Delta\lambda$ was calculated to be ≈ 1.38 Å, with the SE wavelength of $\lambda_{SE} = 1.0615$ μm, which was in good agreement with the experimental value. Finally, Fig. 4 explains the nature of SE studied by showing the $^4F_{3/2} \rightarrow {}^4I_{11/2}$ luminescence spectrum and the corresponding crystal-field

Property	
Space group	$D_{2h}^{14} - Pcam\ (Pbcn)$, No. 60
Unit cell parameters, Å	*Pcam* setting [27]: $a = 5.757$, $b = 14.97$, $c = 5.225$ — *Pbcn* setting [28] [a,b]: $a = 14.926$, $b = 5.752$, $c = 5.204$
Number of formula per unit cell	$Z = 4$
Density, g cm^{-3}	≈ 4.72
Melting temperature, °C [c]	≈ 1560
Site symmetry and coordination numbers (CN) of cations	$Nb^{5+} - C_1$, CN = 6 $Ca^{2+} - C_2$, CN = 8
Method of growth	Czochralski from the melt [17–23], LHPG technique [29] [d], flux [30]
Thermal conductivity, W/m/K [e] [31]	$\kappa_a \approx 6.08$; $\kappa_b \approx 5.71$; $\kappa_c \approx 8.24$
Known Ln^{3+} lasants for $Ca(NbO_3)_2$ host-crystals	Pr^{3+}, Nd^{3+}, Ho^{3+}, Er^{3+}, and Tm^{3+} [17–23]
Possible charge compensators at the Ln^{3+}-doping	Na^+ and Ti^{4+}
Linear optical character	Biaxial, positive
Optical transparency range, μm [f]	$\approx 0.3 - \approx 5.5$
Refractive index	Varies from 2.07 to 2.20 [19]
Hardness (Mohs scale)	4.5 – 5.5
SE effective peak-cross-section, 10^{-20} cm^2	$\sigma_e^p = 12 \pm 5$ [g]
Extension of phonon spectrum, cm^{-1}	≈ 950 [h]
Frequency of SRS-promoting vibration modes, cm^{-1}	$\omega_{SRS1} \approx 904$ and $\omega_{SRS2} \approx 538$
Linewidth (FWHM) of SRS-related peaks in spontaneous Raman scattering spectra, cm^{-1}	$\Delta\nu_{R1} \approx 2.2$ and $\Delta\nu_{R2} \approx 6.5$
First Stokes steady-state Raman gain coefficient, cm/GW	$g_{ssR}^{St1} \approx 2.8$ [i]
Possible applications	Lasers, SRS laser converters, Stokes and anti-Stokes lasing combs, as well as holography [32] and lamp phosphors (Eu^{3+}) [33]

[a] According to a quite recent refinement [34]: $a = 14.96976$; $b = 5.74724$; $c = 5.22202$ Å.
[b] For $Ca(NbO_3)_2$:Pr^{3+}($C_{Pr} \approx 0.5$ at.%) crystal these parameters are: $a = 14.961$; $b = 5.740$; $c = 5.2174$ Å [35].
[c] In the binary system CaO-Nb_2O_5 probably three compounds are formed: the congruently melting orthorhombic methaniobate $Ca(NbO_3)_2$ (at ≈ 1560°C with a ratio 1:1) and monoclinic pyroniobate $Ca_2Nb_2O_7$ (at ≈ 1576°C with a ratio 2:1), and the incongruently melting orthoniobate $Ca_3(NbO_4)_2$ (at ≈ 1535°C with the ratio 3:1) [36].
[d] LHPG – laser heated pedestal growth.
[e] For $Ca(NbO_3)_2$:Nd^{3+} single crystal ($C_{Nd} = 0.894 \times 10^{20}$ cm^{-3}).
[f] For ≈ 1-mm thick plate.
[g] For $^4F_{3/2} \rightarrow {}^4I_{11/2}$ luminescence transitions at 1.0615 μm wavelength related to SE generation line.
[h] From spontaneous Raman scattering spectra.
[i] For the first Stokes SRS line at 1.1741 cm^{-1} wavelength related to $\omega_{SRS1} \approx 904$ cm^{-1}.

Table 3 Some known room-temperature physical properties of the orthorhombic $Ca(NbO_3)_2$ and Nd^{3+}:$Ca(NbO_3)_2$ single crystals

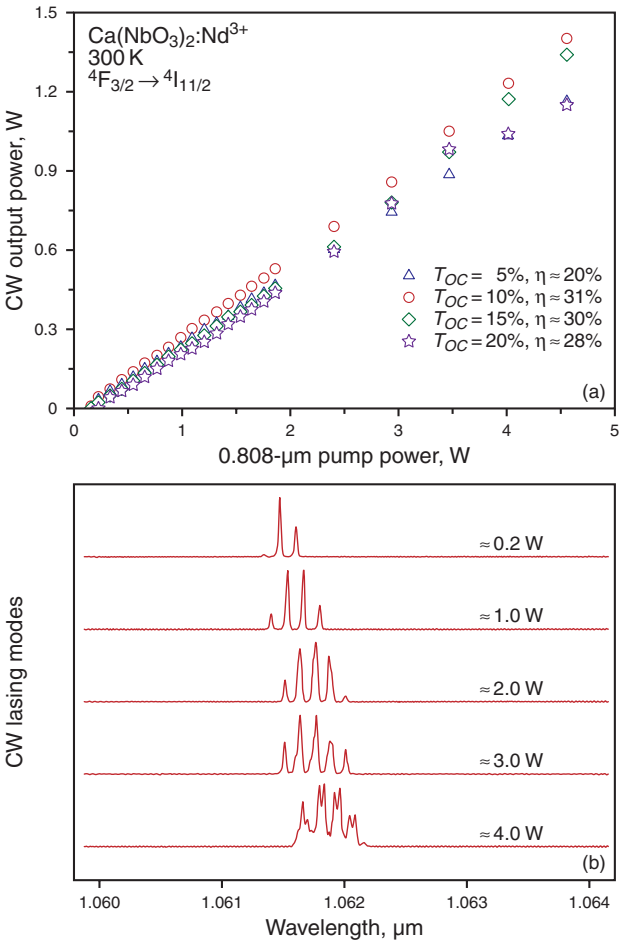

Figure 3 (online color at www.lphys.org) Characteristics of the LD-pumped Nd^{3+}:$Ca(NbO_3)_2$ microchip laser: (a) – output power as a function of 808-μm pump power for different transmissions of the output coupler and (b) – mode-structure of CW lasing spectra for $T_{OC} \approx 10\%$ with indication of pump power (see also text)

splitting scheme with the identification its inter-Stark laser transitions.

4. Raman induced $\chi^{(3)}$-nonlinear Stokes and anti-Stokes lasing

In the conducted room-temperature SRS experiments we used an undoped $Ca(NbO_3)_2$ sample in the form of ≈ 25-mm long rectangular bar (with cross-section 5×5.5 mm^2) whose polished plane-parallel faces were cut perpendicular to the crystallographic c, a, and b axes. Its Raman induced Stokes and anti-Stokes generation in the visible and near-IR spectral regions was excited in the "cavity-free" single-pass pumping geometry by the picosecond radiation of a homemade one micron Nd^{3+}:$Y_3Al_5O_{12}$ laser and double-pass amplifier. Fig. 5 shows only a functional

Excitation condition		Stokes and anti-Stokes generation			SRS-active vibration mode, cm^{-1}	
λ_f, μm	Pumping geometry [a]	Wavelength, μm [b]	Line [c]	SRS- and RFWM-line attribution	ω_{SRS1}	ω_{SRS2}
0.53207	$c(bb)c$ (see Fig. 6a)	0.4650	AST_{3-1}	ω_{f2}+3ω_{SRS1}	≈904	
		0.4854	AST_{2-1}	ω_{f2}+2ω_{SRS1}	≈904	
		0.5077	AST_{1-1}	$\omega_{f2}+\omega_{SRS1}$	≈904	
		0.53207	λ_{f2}	ω_{f2}	–	–
		0.5590	St_{1-1}	$\omega_{f2}-\omega_{SRS1}$	≈904	
		0.5887	St_{2-1}	$\omega_{f2}-2\omega_{SRS1}$	≈904	
		0.6218	St_{3-1}	$\omega_{f2}-3\omega_{SRS1}$	≈904	
		0.6588	St_{4-1}	$\omega_{f2}-4\omega_{SRS1}$	≈904	
		0.7006	St_{5-1}	$\omega_{f2}-5\omega_{SRS1}$	≈904	
1.06415	$c(bb)c$ (see Fig. 6a, Fig. 6c)	0.5703	AST_{9-1}	ω_{f1}+9ω_{SRS1}	≈904	
		0.6014	AST_{8-1}	ω_{f1}+8ω_{SRS1}	≈904	
		0.6359	AST_{7-1}	ω_{f1}+7ω_{SRS1}	≈904	
		0.6747	AST_{6-1}	ω_{f1}+6ω_{SRS1}	≈904	
		0.7185	AST_{5-1}	ω_{f1}+5ω_{SRS1}	≈904	
		0.7685	AST_{4-1}	ω_{f1}+4ω_{SRS1}	≈904	
		0.8258	AST_{3-1}	ω_{f1}+3ω_{SRS1}	≈904	
		0.8925	AST_{2-1}	ω_{f1}+2ω_{SRS1}	≈904	
		0.9708	AST_{1-1}	$\omega_{f1}+\omega_{SRS1}$	≈904	
		1.06415	λ_{f1}	ω_{f1}	–	–
		1.1774	St_{1-1}	$\omega_{f1}-\omega_{SRS1}$	≈904	
		1.3177	St_{2-1}	$\omega_{f1}-2\omega_{SRS1}$	≈904	
		1.4959	St_{3-1}	$\omega_{f1}-3\omega_{SRS1}$	≈904	
		1.7298	St_{4-1}	$\omega_{f1}-4\omega_{SRS1}$	≈904	
1.06415	$c(aa)c$ (see Fig. 7)	0.7185	AST_{5-1}	ω_{f1}+5ω_{SRS1}	≈904	
		0.7685	AST_{4-1}	ω_{f1}+4ω_{SRS1}	≈904	
		0.7921	AST_{6-2}	ω_{f1}+6ω_{SRS2}		≈538
		0.8030	$AST_{4-2}AST_{1-1}$	$\omega_{f1}+\omega_{SRS1}$+4$\omega_{SRS2}$	≈904	≈538
		0.8143	$AST_{2-2}AST_{2-1}$	ω_{f1}+2ω_{SRS1}+2ω_{SRS2}	≈904	≈538
		0.8258 [d]	AST_{3-1}	ω_{f1}+3ω_{SRS1}	≈904	
		0.8273 [d]	AST_{5-2}	ω_{f1}+5ω_{SRS2}		≈538
		0.8393	$AST_{3-2}AST_{1-1}$	$\omega_{f1}+\omega_{SRS1}$+3$\omega_{SRS2}$	≈904	≈538
		0.8516	$AST_{1-2}AST_{2-1}$	ω_{f1}+2$\omega_{SRS1}+\omega_{SRS2}$	≈904	≈538
		0.8659	AST_{4-2}	ω_{f1}+4ω_{SRS2}		≈538
		0.8828	$AST_{2-2}AST_{1-1}$	$\omega_{f1}+\omega_{SRS1}$+2$\omega_{SRS2}$	≈904	≈538
		0.8925	AST_{2-1}	ω_{f1}+2ω_{SRS1}	≈904	
		0.9082	AST_{3-2}	ω_{f1}+3ω_{SRS2}		≈538
		0.9226	$AST_{1-2}AST_{1-1}$	$\omega_{f1}+\omega_{SRS1}+\omega_{SRS2}$	≈904	≈538
		0.9375	$St_{1-2}AST_{2-1}$	ω_{f1}+2$\omega_{SRS1}-\omega_{SRS2}$	≈904	≈538
		0.9548	AST_{2-2}	ω_{f1}+2ω_{SRS2}		≈535
		0.9708	AST_{1-1}	$\omega_{f1}+\omega_{SRS1}$	≈904	
		0.9873	$St_{2-2}AST_{2-1}$	ω_{f1}+2ω_{SRS1}−2ω_{SRS2}	≈904	≈538
		1.0065	AST_{1-2}	$\omega_{f1}+\omega_{SRS2}$		≈538
		1.0243	$St_{1-2}AST_{1-1}$	$\omega_{f1}+\omega_{SRS1}-\omega_{SRS2}$	≈904	≈538
		1.06415	λ_{f1}	ω_{f1}	–	–
		1.1073	$AST_{1-2}St_{1-1}$	$\omega_{f1}-\omega_{SRS1}+\omega_{SRS2}$	≈904	≈538
		1.1288	St_{1-2}	$\omega_{f1}-\omega_{SRS2}$		≈538
		1.1774	St_{1-1}	$\omega_{f1}-\omega_{SRS1}$	≈904	
		1.2018	St_{2-2}	ω_{f1}−2ω_{SRS2}		≈538

[a] Notation is used by analogy to [40].The letters between the parentheses are (from left to right) the polarization of the pumping and nonlinear-laser scattering emission, respectively, while the ones to the left and to the right of the parentheses are the pump and scattered emission detections, respectively. We used crystallographic setting of *Pbcn*, where $a \parallel x$, $b \parallel y$, and $c \parallel z$.

[b] Measurement accuracy is ±0.0003 μm.

[c] For example, the conditional notation $St_{1-2}AST_{2-1}$ if defined as the first Stokes lasing with the second promoted vibration mode ω_{SRS2} from the second anti-Stokes emission with the first promoting vibration mode ω_{SRS2}.

[d] Due to limited resolution of recording monochromator these lines in the spectrum of Fig. 6 are partly overlapped.

Table 4 Room-temperature SRS-promoting modes and spectral composition of Stokes and anti-Stokes generation in undoped orthorhombic $Ca(NbO_3)_2$ single crystal under picosecond Nd^{3+}:$Y_3Al_5O_{12}$-laser pumping at two fundamental wavelengths λ_{f1} = 1.06415 μm and λ_{f2} = 0.53207 μm (SHG)

Symmetry	Overall degree of freedom	Acoustic modes	Translatory lattice modes		Libratory lattice + internal modes of $Nb_2O_6^{2-}$	Activity	
	N	T	$T'(Ca^{2+})$	$T'(Nb^{5+})$	L + i	Raman	IR
A_g	13	–	1	3	9	xx, yy, zz	–
A_u	13	–	1	3	9	–	–
B_{1g}	14	–	2	3	9	xy	–
B_{1u}	14	1	2	3	8	–	z
B_{2g}	13	–	1	3	9	xz	–
B_{2u}	13	1	1	3	8	–	y
B_{3g}	14	–	2	3	9	xz	–
B_{3u}	14	1	2	3	8	–	x
Σ	108	3	12	24	69		

Table 5 Factor-group analysis of the unit-cell vibration modes for $Ca(NbO_3)_2$ single crystal

fragment of the used SRS setup whose detailed description presented in our earlier papers (see, e.g. [39]). The Nd^{3+}:$Y_3Al_5O_{12}$ amplifier is operated at high pump energies to achieve high pulse stability ($\tau_{f1} \approx 110$ ps), therefore the pulse energy variation on the $Ca(NbO_3)_2$ crystal is realized by an attenuator consisting of a half-wave plate along with a Glan-laser polarizer (P). A spherical, plane-convex lens (L_1) with a focal length of 25 cm is used to focus the nearly Gaussian pump beam onto the calcium niobate sample, resulting in a beam waist diameter of about 160 μm. The fundamental pumping wavelength of $\lambda_{f1} = 1.06415$ μm can be converted by SHG in a KTiOPO4 doubler with ≈ 25% efficiency. This results in a pump wavelength of $\lambda_{f2} = 0.53207$ μm and reduced pulse duration of ($\tau_{f2} \approx 80$ ps). A Schott BG39 glass filter with a transmission of 0.015% at 1.064 μm wavelength can be inserted behind the doubler to suppress the fundamental pump radiation of $\lambda_{f1} = 1.06415$ μm. Excitation geometry can be adjusted by a sample stage with three translational and three rotational degrees of freedom. This allows alignment of the $Ca(NbO_3)_2$ sample at any angle with respect to the pump beam direction and polarization. Due to the conical emission characteristics of the Raman induced four-wave mixing (RFWM) in the crystal studied, it is necessary to exploit the complete acceptance angle of the grating spectrometer-monochromator in the Czerny-Turner arrangement (McPherson Model 270, 6.8 Å/pixel dispersion with a grating of 150 lines/mm) used for signal detection. A spherical, bi-convex fused silica lens (L_2) with ≈ 50 mm diameter and 100 mm focal length, followed by a cylindrical plano-convex fused silica lens (L_3) with a size of 50×50 mm^2 and same focal length of 100-mm, images the scattered radiation onto the variable spectrometer entrance slit. For the detection of scattering components emitted at very large angles an additional lens can be inserted behind the sample. This collection geometry is chosen to achieve high sensitivity for different scattering conditions due to different sample properties like size, dispersion and Raman shift, varying positions of the focal plane along the sample length and shifts of the image caused by sample rotation. The spectral components of the collected light are then recorded by a line camera to obtain single shot spectra of wavelengths intervals of up to 0.75 μm width depending on the sensor chip size and the used grating order. For measurements in the UV and visible spectral region a Si-CCD sensor (Hamamatsu S3923-1024Q with 1024 pixels) was used, with peak sensitivity at ≈ 0.6 μm, reduced to almost zero around 1.1 μm wavelength. However for near-IR spectra between 0.9 and 1.7 μm an InGaAs sensor had to be employed (Hamamatsu G9204-512D with 512 Pixels). These sensors provide good enough sensitivity in a very wide spectral range (see, inserted frame in Fig. 6). Some obtained $\chi^{(3)}$-nonlinear lasing spectra of orthorhombic $Ca(NbO_3)_2$ crystal with results of their corresponding analysis are listed in Table 4 and illustrated in Fig. 7 and Fig. 8.

It can be seen from the presented data (see Fig. 6b, Fig. 6c) that in the experimental geometry *c*(*bb*)*c* under one-micron piscosecond pumping in orthorhombic $Ca(NbO_3)_2$ single crystal, a comb of 14 wavelength (4 Stokes and 9 anti-Stokes, and pumping emission) with strictly equally separated lines (by one of SRS-promoting vibration mode $\omega_{SRS1} \approx 904$ cm^{-1}), spanning from the visible ($\lambda_{ASt1-1} = 0.5703$ μm) to the mid-IR region ($\lambda_{St4-1} = 1.7298$ μm), was excited by direct SRS and by parametric RFWM processes. The comb covers a frequency interval of 11754 cm^{-1}, which corresponds to more than two octaves. In the other excitation geometry $c(aa)c$, as will be seen from Fig. 7, the $Ca(NbO_3)_2$ crystal manifests very active $\chi^{(3)}$-nonlinear lasing with two SRS-promoting vibration modes $\omega_{SRS1} \approx 904$ cm^{-1} and $\omega_{SRS2} \approx 538$ cm^{-1}. Moreover, between Stokes and anti-Stokes coherent lasing components that are related to these modes, parametric interactions arise under increasing pumping energy; this gives rise to strong cascade $\chi^{(3)} \leftrightarrow \chi^{(3)}$ generation. As a result, the "conglomeration"

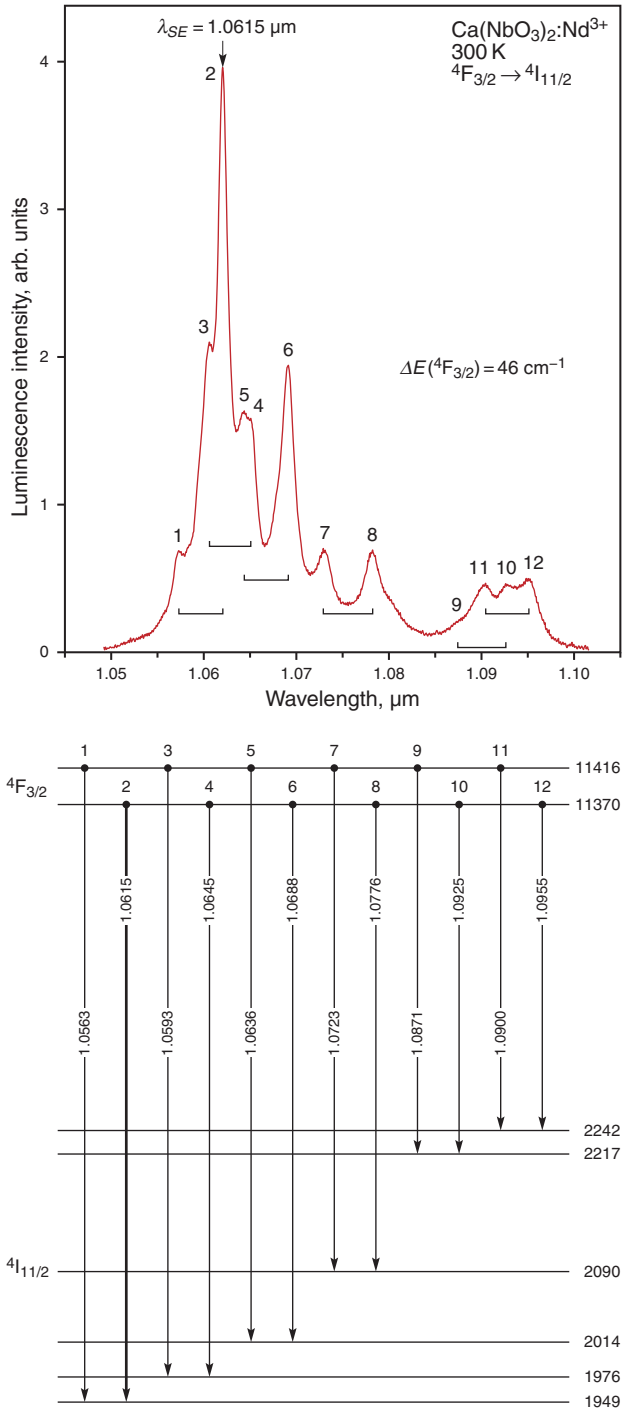

Figure 4 (online color at www.lphys.org) Room-temperature luminescence spectrum ($^4F_{3/2} \rightarrow {}^4I_{11/2}$ channel) and crystal-field splitting scheme of the $^4F_{3/2}$ and $^4I_{11/2}$ manifolds of Nd^{3+} ions in orthorhombic $Ca(NbO_3)_2$ crystal. Energies of Stark levels are given in cm^{-1}, and transitions between them are shown in μm. Here, the thick arrow shows the laser transition. Lines in the spectrum and inter-Stark transitions in the energy scheme are denoted by corresponding numbers to facilitate their comparison. The square brackets in the spectrum show the splitting ($\Delta E(^4F_{3/2}) = 46$ cm^{-1}) of the initial laser $^4F_{3/2}$ state

Excitation geometry [a]			Assignment [b]	
A_g z(xx)z	A_g z(yy)z	A_g y(zz)y		
950 vw	950 vw	950 vw		
904 vs	904 vs	904 vs	ν_1	$\nu(NbO_t)$
	846 w	846 vw		
	657 vw	657 vw	ν_2	$\nu(NbO_b)$
538 s	538 m	538 w	ν_3	$\nu(NbO_b)+\nu(CaO)$
480 w	480m	480 w	ν_4	$\nu(NbO_c)$
	425 w	425 vw		
	380 s	380 w	ν_5	$\delta(ONbO)+\nu(NbO_c)$
287 m		287 m	ν_6	$\delta(ONbO)+\nu(NbO_c)$
282 m	282 m		ν_7	$\delta(ONbO)+\nu(CaO)$
	257 w	257 w		
236 m	236 s	236 m	ν_8	$\delta(ONbO)+\nu(CaO)$
220 m	220 vw	220 vw	ν_9	$T'(Ca^{2+})+\delta(ONbO)$
190 m		190 m	ν_{10}	$\delta(ONbO)+T'(Ca^{2+})$
		160 vw		
134 m	134 m	134 vw	ν_{11}	$T'(Nb^{5+})$
			ν_{12}	$T'(Nb^{5+})$
60 w	60 w		ν_{13}	$T'(Nb^{5+})$

[a] Here $a \| x$, $b \| y$, and $c \| z$.
[b] O_t – terminal oxygen, O_b – bridging oxygen, and O_c – chain oxygen.

Table 6 Raman wavenumbers of $Ca(NbO_3)_2$ single crystals

of interconnected Stokes and anti-Stokes lasing lines becomes more condensed. The physical nature of this interesting nonlinear-laser phenomenon necessitates a special examination, as analogous effects were already observed in several inorganic and organic crystals with different structures, offering more than one SRS-promoting vibrational modes (see, for example, β'-$Gd_2(MoO_4)_3$ [41], α-$KY(WO_4)_2$ and α-$KGd(WO_4)_2$ [42], $C_{13}H_{10}O$ [43], $Li_2B_4O_7$ [44], $(NH_3CH_2CH_2NH_3)\{(+)\text{-}C_4H_4O_6\}$ [45], $GdVO_4$ [46], YPO_4 [47], $LaBO_2MoO_4$ [48], etc.).

For the undoped $Ca(NbO_3)_2$ crystal we can also roughly estimate the steady-state (SS) Raman gain coefficient for its first Stokes lasing component $\lambda_{St1-1} = 1.1774$ μm, which related to the SRS-promoting vibration mode $\omega_{SRS1} \approx 904$ cm^{-1}. The used pumping conditions allowed to perform this evaluation because $\tau_{f1} \gg T_2 = (\pi \Delta\nu_{R1}) \approx 4.8$ ps (here T_2 is the dephasing time of vibration mode and $\Delta\nu_{R1} \approx 2.2$ cm^{-1} is the linewidth of its Raman shifted line in spontaneous Raman scattering spectrum (see, Fig. 8c). This was done indirectly by the sufficiently tested method based on the well known ratio $g_{ssR}^{St1-1} I_p^{thr} l_{SRS} \approx 30$ (see, e.g. [49]) and a comparison of the "threshold" pump intensity (I_p^{thr}) of the confidently measurable lasing signal at $\lambda_{St1-1} = 1.1774$ μm wavelength for the studied calcium niobate and reference crystal $PbWO_4$ with the same SRS-active length ($l_{SRS} \approx 25$ mm)

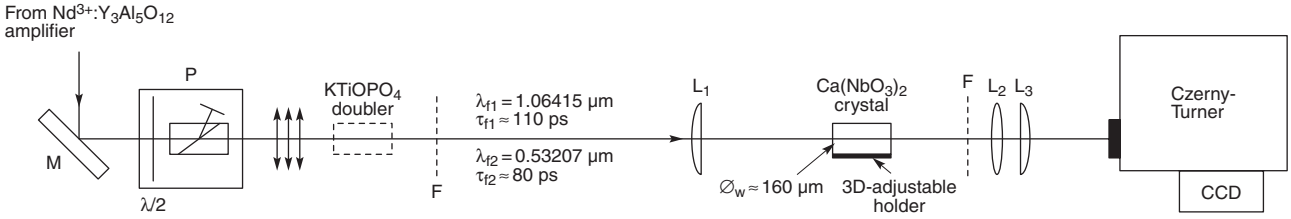

Figure 5 (online color at www.lphys.org) Schematic fragment of SRS laser setup (see also text)

and known value $g_{ssR}^{St1} = 3.1 \pm 0.8$ cm/GW [50] for its $\lambda_{St1-1} = 1.1770$ μm component. We found that the required first-Stokes "threshold" intensity of $Ca(NbO_3)_2$ crystal was about 10% larger than for the reference lead tungstate. This result allows us conclude that the desired value of g_{ssR}^{St1-1} coefficient for the first Stokes lasing at $\lambda_{St1-1} = 1.1774$ μm wavelength of orthorhombic calcium niobate is not less than 2.8 cm/GW.

5. Symmetry based vibrational characteristics of the crystal, SRS-promoting modes

The structure of the $Ca(NbO_3)_2$ is described as mentioned above by the D_{2h}^{14} orthorhombic space group with $Z = 4$. The unit cell consists of 8 Nb, 4 Ca, and 24 oxygen atoms. Eight niobium atoms occupy the $8d$ positions with C_1 symmetry (see, also Table 3), each of them coordinated to the six oxygen atoms. The NbO_6 units form chains of octahedra joined together at their edges along the c-axis (see Fig. 1 in [32]). Two chains are linked together by their corners but the double chains are coupled through the calcium cations. Four calcium atoms occupy the $4e$ positions with C_2 symmetry. Each Ca^{2+} ion is surrounded by 8 oxygen atoms giving two sets of equivalent Ca-O bonds in an irregular cuboid. All three non-equivalent oxygen atoms of the unit cell occupy the $8d$ position with C_1 symmetry.

The D_{2h}^{14} orthorhombic unit cell of the $Ca(NbO_3)_2$ crystal comprises 36 atoms that have 108 zone-center (at $\mathbf{k} = 0$) degrees of freedom described by the irreducible representations Γ_{108}=13A_g+13A_u+14B_{1g}+14B_{1u}+13B_{2g}+13B_{2u}+14B_{3g}+14B_{3u} of to following origin:

$\Gamma(Ca^{2+})$: A_g+A_u+2B_{1g}+2B_{1u}+B_{2g}+B_{2u}+2B_{3g}+2B_{3u};
$\Gamma(Nb^{5+})$: 3A_g+3A_u+3B_{1g}+3B_{1u}+3B_{2g}+3B_{2u}+3B_{3g}+3B_{3u};
$\Gamma(O_t^{2-})$: 3A_g+3A_u+3B_{1g}+3B_{1u}+3B_{2g}+3B_{2u}+3B_{3g}+3B_{3u};
$\Gamma(O_b^{2-})$: 3A_g+3A_u+3B_{1g}+3B_{1u}+3B_{2g}+3B_{2u}+3B_{3g}+3B_{3u};
$\Gamma(O_c^{2-})$: 3A_g+3A_u+3B_{1g}+3B_{1u}+3B_{2g}+3B_{2u}+3B_{3g}+B_{3u}.

Three of the unit cell phonons, $\Gamma_T = B_{1u}+B_{2u}+B_{3u}$, describe the acoustic modes and the remaining, Γ_o=13A_g+13A_u+14B_{1g}+13B_{1u}+13B_{2g}+12B_{2u}+14B_{3g}+13B_{3u} correspond to the optical modes. The optical phonons can be further subdivided into:

– translational lattice phonons of Ca^{2+} ions:
$\Gamma_{T'}(Ca^{2+})$=A_g+A_u+2B_{1g}+2B_{1u}+B_{2g}+B_{2u}+2B_{3g}+2B_{3u};
– translational lattice phonons of Nb^{5+} ions:
$\Gamma_{T'}(Nb^{5+})$=3A_g+3A_u+3B_{1g}+3B_{1u}+3B_{2g}+3B_{2u}+3B_{3g}+3B_{3u};
– internal (stretching and bending) and librational lattice phonons of the NbO_6 octahedral units:
Γ_{i+L}=9A_g+9A_u+9B_{1g}+8B_{1u}+9B_{2g}+8B_{2u}+9B_{3g}+8B_{3u}.

Table 5 presents the results of the factor-group analysis for the unit-cell phonons of the crystal studied and their IR and Raman activities. The coupling of the librational and bending modes of the NbO_6 units should be taken into account in the factor-group approach because they form ribbon of octahedrs joined together at their edges. Therefore the librational motions are frozen and strongly mixed with bending phonons.

The structure of orthorhombic $Ca(NbO_3)_2$ has been studied in a few papers (see, e.g. [51,52]). However, a full analysis of the polarized spectra of this crystal based on the factor-group analysis has not been performed yet. The A_g spontaneous Raman scattering spectra for the $Ca(NbO_3)_2$ are shown in Fig. 8. The wavenubers of the Raman shifted lines are listed in Table 6 together with their tentative assignment to the respective normal modes. The description of the modes has been related to the nomenclature introduced from the normal coordinate analysis in [52]. A few main conclusions can be drawn from the analysis of the A_g-spectra of the orthorhombic $Ca(NbO_3)_2$ crystal:

– nine A_g stretching modes as well as bending modes coupled with the librational motions are observed at following wavenumbers: $\nu_1 = 904$, $\nu_2 = 657$, $\nu_3 = 538$, $\nu_4 = 480$, $\nu_5 = 380$, $\nu_6 = 287$, $\nu_7 = 282$, $\nu_8 = 236$, and $\nu_{10} = 190$ cm^{-1}. The assignment of these modes to respective motions of the niobate chain is presented in Table 6. It is based on the main contribution of these internal coordinates into the normal mode;
– the lattice bands of the $Ca(NbO_3)_2$ crystal appear below 236 cm^{-1}. They correspond to the Ca^{2+} ion translation: $\nu_9 = 220$ cm^{-1} – $T'(Ca^{2+})$ and Nb^{5+} ion translation $\nu_{11} = 134$ cm^{-1} – $T'(Nb^{5+})$. Two other translational phonons of the Nb^{5+} ions: ν_{12} and ν_{13} lie below ≈ 60 cm^{-1}, i.e. in a region not measurable with the used Bruker FT 100/s spectrometer;
– among the modes observed in the fully symmetric A_g-Raman spectra the strogest line appears at 904 cm^{-1} corresponding to the symmetric $\nu(NbO_t)$ mode that is

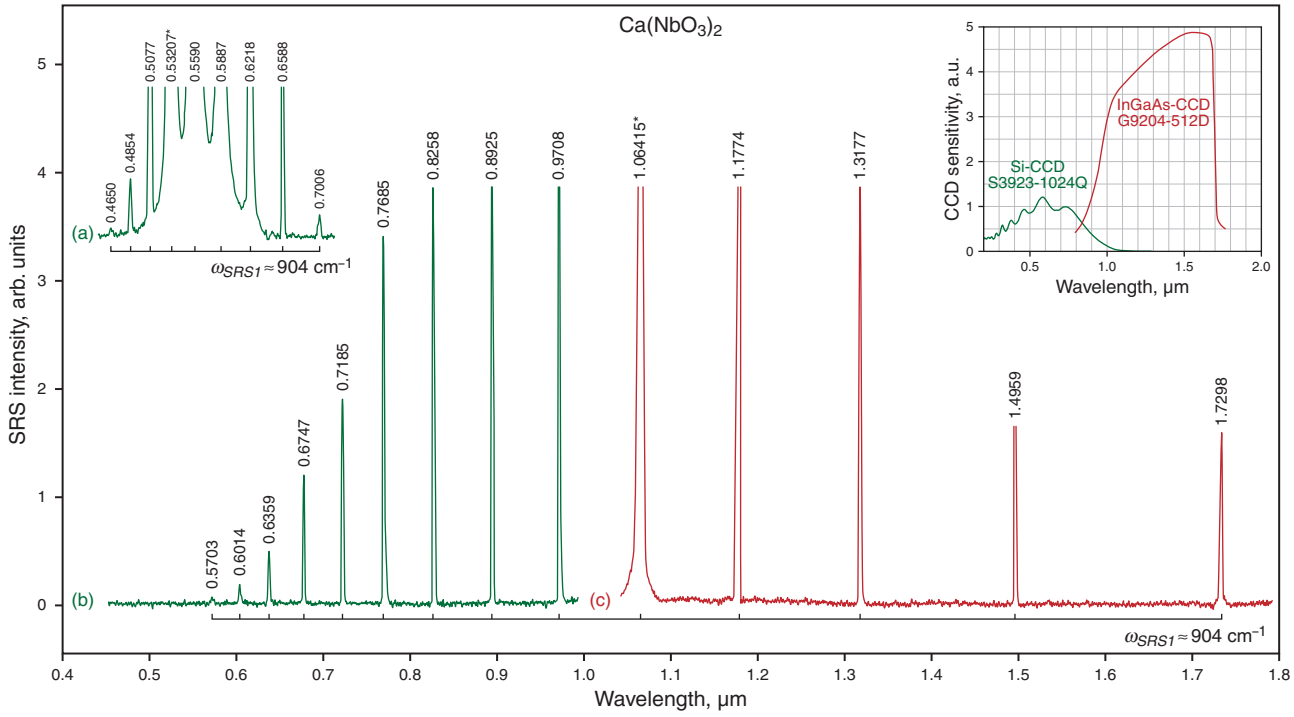

Figure 6 (online color at www.lphys.org) Room-temperature $\chi^{(3)}$-Raman-induced SRS and RFWM lasing spectra of orthorhombic $Ca(NbO_3)_2$ single crystal recorded in excitation geometry $c(bb)c$ with picosecond pumping at $\lambda_{f1} = 1.06415$ μm (see (b) and (c) fragments) and $\lambda_{f2} = 0.53207$ μm wavelength (a). Spectral intensities and wavelength of all lines (pump lines are asterisked) are shown without correction for the spectral sensitivity of used analyzing system with two CCD detectors (shown in the frame). The spectra (a) and (b) were recorded with a Si-CCD, spectrum (c) with an InGaAs-CCD array sensor. The spacing of the Stokes and anti-Stokes lasing components is a multiple of the single SRS-promoting vibration mode with $\omega_{SRS1} \approx 804$ cm^{-1} of the studied crystal and is indicated by the horizontal scale brackets

the SRS-promoting vibration (ω_{SRS1}). The nature of the second SRS-promoting mode ($\omega_{SRS2} \approx 538$ cm^{-1}) is related to the complex stretching and bonding vibration $\nu(NbO_b) + \nu(CaO)$.

6. Conclusion

From the results of this research it can be concluded that undoped orthorhombic $Ca(NbO_3)_2$ crystal is a promising $\chi^{(3)}$-active material for Raman laser converters in the visible and near-IR regions, as well as for picosecond generation of high-order Stokes and anti-Stokes comb covering more than two octaves lasing wavelengths. This crystal offering two SRS-promoting vibration modes is also an attractive candidate to investigate the cross-cascade ($\chi^{(3)} \leftrightarrow \chi^{(3)}$)-nonlinear parametric interactions which "closely interlink" these modes. The experiments carried out with the Nd^{3+}:$Ca(NbO_3)_2$ crystal have confirmed earlier laser results that this SE-active material is suitable to develope different type solid-state lasers, in particular we achieved on its base an efficient CW microchip. Due to the rather high measured main SE and SRS lasing characteristics of the crystals studied (effective peak-cross section $\sigma_e^p = (12\pm5)\times10^{-20}$ cm^2 for the SE transition at $\lambda_{SE} = 1.0615$ μm wavelength of the $^4F_{3/2} \rightarrow {}^4I_{11/2}$ lasing channel of Nd^{3+} ions and steady-state first-Stokes Raman gain coefficient $g_{ssR}^{Sti1-1} \approx 2.8$ cm/GW for $\chi^{(3)}$-lasing at $\lambda_{St1-1} = 1.1774$ μm wavelength related to SRS-promoting vibration mode $\omega_{SRS1} \approx 904$ cm^{-1} of $Ca(NbO_3)_2$ crystal) we could develop a nanosecond Nd^{3+}:$Ca(NbO_3)_2$ self-Raman laser with LD pumping. These results will be reported in a following paper.

Acknowledgements The authors are obliged to note that the research reported here was considerably advanced by the cooperation with the "Joint Open Laboratory for Laser Crystals and Precise Laser Systems". The authors thank for partial support the Institute for Low Temperature and Structure Research of the Polish Academy of Sciences, the Technical University of Berlin, the Xiamen University, the Tokyo University of Electro-Communications, and the University of Verona. One of us (A.A.K.) acknowledges the partial financial support from the Russian Foundation for Basic Research and the Program of the Presidium of Russian Academy of Sciences "Extreme laser fields and their applications", as well as he is grateful also to the Alexander von Humboldt Foundation for the "Festkörperphysik" Research Prize, which allowed him to carry out SRS experiments

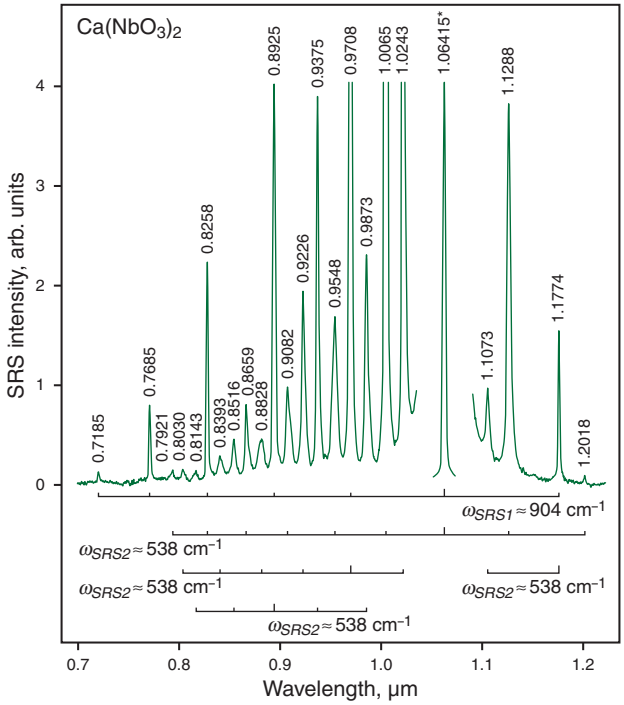

Figure 7 (online color at www.lphys.org) Room-temperature $\chi^{(3)}$-Raman-induced SRS and RFWM lasing spectra of orthorhombic $Ca(NbO_3)_2$ single crystal recorded in excitation geometry $c(aa)c$ with picosecond pumping at $\lambda_{f1} = 1.06415$ μm wavelength. The spacing of the Stokes and anti-Stokes lasing components is a multiple of two SRS-promoting vibration modes with $\omega_{SRS1} \approx 904$ cm^{-1} and $\omega_{SRS2} \approx 538$ cm^{-1} are indicated by the horizontal scale brackets. Other notations as in Fig. 6

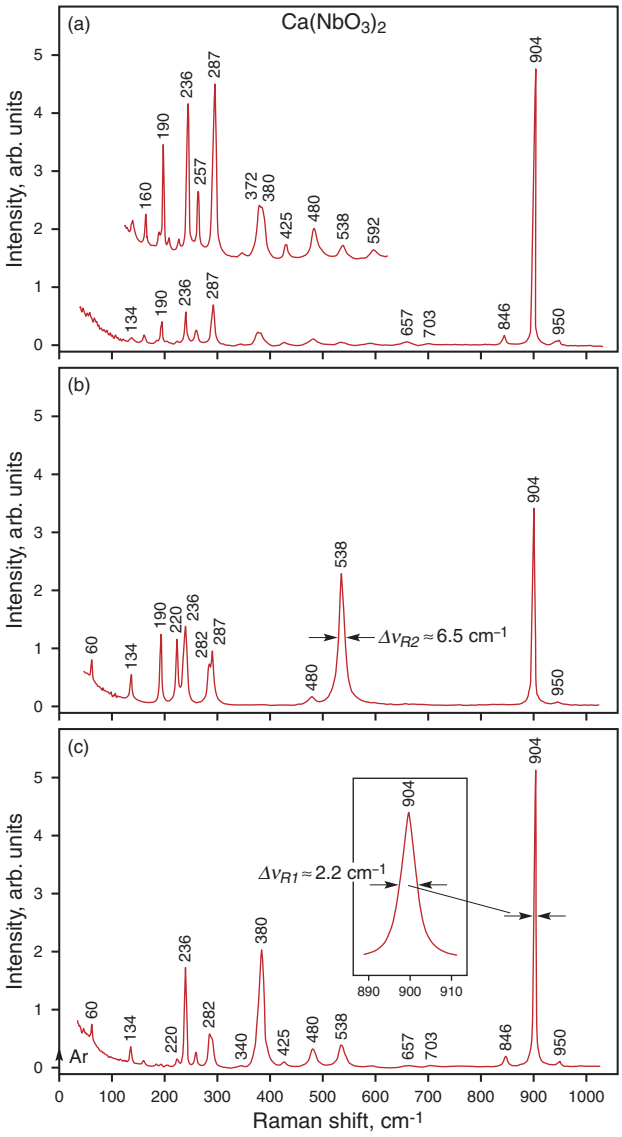

Figure 8 (online color at www.lphys.org) Room-temperature polarized spontaneous Raman scattering A_g-spectra for the orthorhombic $Ca(NbO_3)_2$ single crystal recorded in excitation geometries: (a) – $b(cc)b$, (b) – $c(aa)c$, and (c) – $c(bb)c$ under excitation of Ar-ion laser at 0.488 μm wavelength (shown by the arrow). Some Raman shifted lines are given in cm^{-1}. The linewidths $\Delta\nu_R$ are indicated only for the lines related to SRS-promoting vibrational transitions of the crystal

at the Institute of Optics and Atomic Physics of the Technical University of Berlin.

References

[1] M.J. Weber (ed.), CRC Handbook of Laser Science and Technology, suppl. 1: Lasers (CRC Press, Boca Raton, 1995).

[2] A.A. Kaminskii, Crystalline Lasers: Physical Processes and Operating Schemes (CRC Press, Boca Raton, 1996).

[3] V.G. Dmitriev, G.G. Gurzadyan, and D.N. Nikogosyan, Handbook of Nonlinear Optical Crystals (Springer, Berlin, 1997).

[4] C.E. Webb and J.D.C. Jones (eds.), Handbook of Laser Technology and Applications, vol. 2 (Institute of Physics, London, 2003).

[5] H.M. Pask, P. Dekker, R.P. Mildren, D.J. Spence, and J.A. Piper, Prog. Quantum Electron. **32**, 121 (2008).

[6] W.D. Johnston, Jr., I.P. Kaminow, and J.G. Bergman, Jr., Appl. Phys. Lett. **13**, 190 (1969); J. Gelbwachs, R.H. Pantell, H.E. Puthoff, and J.M. Yarborough, Appl. Phys. Lett. **14**, 258 (1969); J.M. Yarborough, S.S. Sussman, H.E. Puthoff, R.H. Pantell, and B.C. Johnson, Appl. Phys. Lett. **15**, 102 (1969).

[7] A.A. Kaminskii, H.J. Eichler, D. Grebe, R. Macdonald, J. Findeisen, S.N. Bagayev, A.V. Butashin, A.F. Konstantinova, H. Manaa, R. Moncorge, F. Bourgeois, and G. Boulon, Opt. Mater. **10**, 269 (1998).

[8] A.A. Kaminskii, P. Becker, L. Bohatý, H.J. Eichler, A.N. Penin, K. Ueda, J. Hanuza, K. Takaichi, and H. Rhee, Phys. Status Solidi (a) **201**, 2154 (2004).

[9] A.A. Kaminskii, H.J. Eichler, K. Ueda, J. Fernandez, J. Findeisen, and R. Balda, Quantum Electron. **28**, 939 (1998).

[10] A.A. Kaminskii, D. Jaque, S.N. Bagaev, K. Ueda, J. Garcia-Sole, and J. Copmany, Quantum Electron. **29**, 95 (1998).
[11] A.A. Kaminskii, Crystalline Lasers: Physical Processes and Operating Schemes (CRC Press, Boca Raton, FL, 1996); A.A. Kaminskii, Phys. Status Solidi (a) **200**, 215 (2003); M.J. Weber, Laser Wavelengths (CRC Press, Boca Raton, 2001).
[12] K.G. Belabaev, A.A. Kaminskii, and S.E. Sarkisov, Phys. Status Solidi (a) **28**, K17 (1975).
[13] J. Capmany, E. Montoya, V. Bermúdez, D. Callejo, E. Diéguez, and L.E. Bausá, Appl. Phys. Lett. **76**, 1374 (2000).
[14] A.A. Kaminskii, J. García Solé, S.N. Bagayev, D. Jaque, and J. Capmany, Quntum Electron. **28**, 1031 (1998); J.J. Romero, D. Jaque, J. García Solé, and A.A. Kaminskii, Appl. Phys. Lett. **78**, 1961 (2001).
[15] E.Yu. Morozov, A.A. Kaminskii, A.S. Chirkin and D.B. Yusupov, JETP Lett. **73**, 647 (2001).
[16] A.A. Kaminskii, A.P. Shkadarevich, B.V. Mill', V.G. Loptev, A.V. Butashin, and A.A. Demidivich, Inorg. Mater. **24**, 690 (1986); A.A. Kaminskii, A.V. Butashin, A.A. Demidivich, V.G. Koptev, B.V. Mill, and A.P. Shkadarevich, Phys. Status Solidi (a) **112**, 197 (1989); A.A. Kaminskii, A.V. Butashin, M.I. Demchuk, V.I. Zhavoronkov, V.P. Mikhailov, and A.P. Shkadarevich, Inorg. Mater. **24**, 2075 (1988).
[17] A.A. Kaminskii, Phys. Status Solidi (a) **125**, K109 (1991).
[18] A.A. Kaminskii, G.I. Rogov, and Kh.S. Bagdasarov, Phys. Status Solidi **31**, K87 (1969).
[19] A.A. Ballman, S.P.S. Porto, and A.Yariv, J. Appl. Phys. **34**, 3155 (1963).
[20] A.A. Kaminskii, A.G. Petrosyan, and K.L. Ovanesyan, Phys. Status Solidi (a) **83**, K159 (1984).
[21] A.A. Kaminskii, Phys. Status Solidi (a) **1**, 573 (1970).
[22] A.A. Kaminskii and L. Li, Inorg. Mater. **6**, 254 (1970).
[23] A.A. Kaminskii, S.E. Sarkisov, and L. Li, Phys. Status Solidi (a) **15**, K141 (1973).
[24] V.L. Bakumenko, G.S. Kozina, T.A. Kostinskaya, E.P. Lupachev, and E.S. Rvacheva, Optika i Spektroskopiya **19**, 132 (1965).
[25] A.A. Kaminskii, JETP Lett. **7**, 201 (1968).
[26] A.A. Kaminskii and V.V. Osiko, Inorg. Mater. **1**, 1853 (1965); R.J. Pressly (ed.), CRC Handbook of Lasers, with Selected data on Optical Technology, (CRC Press, Cleveland, 1971); A.A. Kaminskii, Laser Crystals, Their Physics and Properties (Springer, Berlin, 1990).
[27] K.S. Alexandrov, Dokl. Akad. Nauk SSSR **132**, 660 (1960).
[28] H.D. Hess and H.J. Trumpour, Am. Mineral. **44**, 1 (1959).
[29] A.S.S. De Camargo, R. Almeida Silva, J.P. Andreeta, and L.A.O. Nunes, Appl. Phys. B **80**, 497 (2005); R. de Almeida Silva, A.S.S. de Camargo, C. Cusatis, L.A.O. Nunes, and J.P. Andreeta, J. Crystal Growth **262**, 246 (2004).
[30] S. Oishi, Y. Nagai, and N. Ishizawa, Nippon Kagaku Kaishi **9**, 598 (1998), in Japanese.
[31] Y. Cheng, X.D. Xu, J. Xu, Z. Xin, and S.M. Zhou, Appl. Phys. B **96**, 43 (2009).
[32] J.P. Cummings and S.H. Simonsen, Am. Mineral. **55**, 90 (1970).
[33] D. van der Voort, J.M.E. de Ruk, and G. Blasse, Phys. Status Solidi (a) **135**, 621 (1993).
[34] J. Leitner, K. Růžička, D. Sedmidubský, and P. Svoboda, J. Therm. Anal. Calorim. **95**, 397 (2009).
[35] L. Macalik, M. Mączka, J. Hanuza, P. Godlewska, P. Solarz, W. Ryba-Romanowski, and A.A. Kaminskii, J. Alloys Compd. **451**, 232 (2008).
[36] M. Ibrahim, N.F.H. Bright, and J.F. Rowland, J. Am. Ceram. Soc. **45**, 329 (1962).
[37] J. Dong, A. Rapaport, M. Bass, and K. Ueda, Phys. Status Solidi (a) **202**, 2565 (2005).
[38] W. Koechner, Solid State Laser Engineering (Springer, Berlin, 1999).
[39] A.A. Kaminskii, L. Bohatý, P. Becker, H.J. Eichler, and H. Rhee, Physics-Uspekhi **51**, 899 (2008); A.A. Kaminskii, V.V. Dolbinina, H. Rhee, H.J. Eichler, K. Ueda, K. Takaichi, A. Shirakawa, M. Tokurakawa, J. Dong, and D. Jaque, Laser. Phys. Lett. **5**, 532 (2008); A.A. Kaminskii, L. Bohatý, P. Becker, J. Liebertz, P. Held, H.J. Eichler, H. Rhee, and J. Hanuza, Laser Phys. Lett. **5**, 845 (2008); A.A. Kaminskii, L. Bohatý, P. Becker, P. Held, H. Rhee, H.J. Eichler, and J. Hanuza, Laser Phys. Lett. **6**, 335 (2009).
[40] T.C. Damen, S.P.S. Porto, and B. Tell, Phys. Rev. **142**, 570 (1966).
[41] A.A. Kaminskii, A.V. Butashin, H.-J. Eichler, D. Grebe, R. Macdonald, K. Ueda, H. Nishioka, W. Odajima, M. Tateno, J. Song, M. Musha, S.N. Bagaev, and A.A. Pavlyuk, Opt. Mater. **7**, 59 (1997).
[42] A.A. Kaminskii, A.F. Konstantinova, V.P. Orekhova, A.V. Butashin, R.F. Klevtsova, and A.A. Pavlyuk, Crystallogr. Rep. **46**, 665 (2001).
[43] A.A. Kaminskii, H. Klapper, J. Hulliger, H.J. Eichler, J. Hanuza, K. Ueda, K. Takaichi, C. Wickleder, G.M.A. Gad, and M. Maczka, Laser Phys. **12**, 1041 (2002).
[44] A.A. Kaminskii, L. Bohatý, P. Becker, J. Liebertz, H.J. Eichler, and H. Rhee, Laser Phys. Lett. **3**, 519 (2006).
[45] A.A. Kaminskii, L. Bohatý, P. Becker, H.J. Eichler, H. Rhee, M. Maczka, and J. Hanuza, Laser Phys. Lett. **4**, 291 (2007).
[46] A.A. Kaminskii, H.J. Eichler, and H. Rhee, Cryst. Res. Technol. **43**, 1117 (2008).
[47] A.A. Kaminskii, M. Bettinelli, A. Speghini, H. Rhee, H.J. Eichler, and G. Mariotto, Laser. Phys. Lett. **5**, 367 (2008).
[48] P. Becker, L. Bohatý, H. Rhee, H.J. Eichler, J. Hanuza, and A.A. Kaminskii, Laser Phys. Lett. **5**, 114 (2008).
[49] W. Kaiser and M. Maier, in: F.T. Arichi and E.O. Schultz-Dubois (eds.), Laser Handbook, vol. 2 (North-Holland, Amsterdam, 1972), p. 1077; Y.R. Shen, The Pronciples of Nonlinear Optics (Wiley, New York, 1984).
[50] A.A. Kaminskii, C.L. McCray, H.R. Lee, S.W. Lee, D.A. Temple, T.H. Chyba, W.D. Marsh, J.C. Barnes, A.N. Annanenkov, V.D. Legun, H.J. Eichler, G.M.A. Gad, and K. Ueda, Opt. Commun. **183**, 277 (2000).
[51] C. Rocchiccili-Deltcheff, T. Dupius, and C. Wadier, C.R. Acad. Sci., Ser. IIb **237**, 1020 (1971); E. Husson, Y. Repelin, N.Q. Dao, and H. Brusset, Spectrochim. Acta, Part A **33**, 995 (1977).
[52] E. Husson, Y. Repelin, N.Q. Dao, and H. Brusset, J. Chem Phys. **66**, 5173 (1977).